Iterative three-dimensional expectation maximization restoration of single photon emission computed tomography images: Application in striatal imaging

Pierre Gantet and Pierre Payoux
Laboratoire de Biophysique EA3033, Université Paul Sabatier, Toulouse, France

Anna Celler
Division of Nuclear Medicine, Vancouver Hospital and Health Sciences Centre, Vancouver, British Columbia, Canada

Cynthia Majorel
Laboratoire de Biophysique EA3033, Université Paul Sabatier, Toulouse, France

Daniel Gourion
Laboratoire d'Analyse non linéaire et de géométrie, Faculté des sciences, Avignon, France

Dominikus Noll
Mathématiques pour l'Industrie et la Physique, Université Paul Sabatier, Toulouse, France

Jean-Paul Esquerré
Laboratoire de Biophysique EA3033, Université Paul Sabatier, Toulouse, France

(Received 1 April 2005; revised 17 October 2005; accepted for publication 17 October 2005; published 20 December 2005)

Single photon emission computed tomography imaging suffers from poor spatial resolution and high statistical noise. Consequently, the contrast of small structures is reduced, the visual detection of defects is limited and precise quantification is difficult. To improve the contrast, it is possible to include the spatially variant point spread function of the detection system into the iterative reconstruction algorithm. This kind of method is well known to be effective, but time consuming. We have developed a faster method to account for the spatial resolution loss in three dimensions, based on a postreconstruction restoration method. The method uses two steps. First, a noncorrected iterative ordered subsets expectation maximization (OSEM) reconstruction is performed and, in the second step, a three-dimensional (3D) iterative maximum likelihood expectation maximization (ML-EM) *a posteriori* spatial restoration of the reconstructed volume is done. In this paper, we compare to the standard OSEM-3D method, in three studies (two in simulation and one from experimental data). In the two first studies, contrast, noise, and visual detection of defects are studied. In the third study, a quantitative analysis is performed from data obtained with an anthropomorphic striatal phantom filled with 123-I. From the simulations, we demonstrate that contrast as a function of noise and lesion detectability are very similar for both OSEM-3D and OSEM-R methods. In the experimental study, we obtained very similar values of activity-quantification ratios for different regions in the brain. The advantage of OSEM-R compared to OSEM-3D is a substantial gain of processing time. This gain depends on several factors. In a typical situation, for a 128×128 acquisition of 120 projections, OSEM-R is 13 or 25 times faster than OSEM-3D, depending on the calculation method used in the iterative restoration. In this paper, the OSEM-R method is tested with the approximation of depth independent resolution. For the striatum this approximation is appropriate, but for other clinical situations we will need to include a spatially varying response. Such a response is already included in OSEM-3D. © *2006 American Association of Physicists in Medicine*. [DOI: 10.1118/1.2135908]

Key words: SPECT, resolution correction, restoration, deconvolution, striatal imaging

I. INTRODUCTION

Several factors contribute to degradation of the spatial resolution in single photon emission computed tomography (SPECT). The most important is the spatial resolution of the imaging system and consists of two independent sources of blurring. The first part, which does not depend on the object-to-collimator distance, is related to the intrinsic resolution of the detector and electronics and may be modeled by a Gaussian distribution. The second is caused by the distance-dependent acceptance of photons through the holes of the collimator.[1] Additional degradation of resolution may be related to image reconstruction method, data and image sampling (partial volume effect), and filtering.

The main effects of poor spatial resolution manifest themselves as image blurring, and quantitative errors in the measured activity of small objects.[2–5] Three classes of methods have been proposed to correct for SPECT collimator blurring problem:

(1) The first class tries to correct or modify the emission data prior to reconstruction, using stationary,[6–9] or nonstationary,[10–12] filtering of the projections. Alternatively, the frequency-distance relationship may be used to take into account the depth-dependent loss of resolution.[13–16] These methods have been used mostly in conjunction with the filtered back projection reconstruction algorithm.
(2) The methods of the second type incorporate the correction directly into the image reconstruction process. A point spread function (PSF) of the camera system is computed at each point of the reconstructed area at each projection angle, and is included into the projection/backprojection operator in the iterative reconstruction process. This modeling may be made in two dimensions, by neglecting the interslice blur, but for the best results calculations should be done in three dimensions.[17–21] Additionally, the projection/backprojection operator pair may be symmetric, or asymmetric.[22,23]
(3) The third class of methods tries to restore the contrast of the image after the reconstruction process. Deconvolution methods using Wiener, Metz, or power spectrum equalization filtering have been initially used in two dimensions by neglecting the interslice blurring,[7] but the three–dimensional (3D) filtering gives better results.[24] A few studies have used iterative methods. Webb *et al.*[25] used entropy maximization to restore two-dimensional (2D) slices of liver. More recently, a blind deconvolution technique, where the 3D PSF was directly estimated from the observed input images, has been proposed.[26]

All these correction methods improve contrast of the reconstructed images. Unfortunately, filtering methods of the first and third class may also substantially increase high frequency noise. To compensate for this effect one needs to use a low pass filter, which again degrades image resolution. On the other hand, the second type of method that accounts for the collimator blurring effect in an iterative reconstruction algorithm based, for example, on the maximum likelihood expectation maximization (ML-EM) method,[27] or its accelerated version [ordered subsets expectation maximization (OSEM)],[28] has a regularizing effect on the reconstructed image. Compared to a reconstruction without blurring correction, high frequency noise is reduced, while contrast is enhanced.

Some studies have shown that the OSEM-3D method using only a few iterations gave better results for the task of detection and localization compared to filtered backprojection.[29,30] The major drawback of these methods is the long computation time required for reconstruction; nevertheless, we will use the OSEM-3D approach as the benchmark against which the method proposed in this paper will be compared. Our method belongs to the third class: it uses an iterative 3D spatial Restoration to be applied after the initial reconstruction of the image.

In this paper, we present our restoration method and compare it to the standard OSEM-3D method in three studies: two using simulations and one based on experimental data. The first study analyzes the contrast and the noise level of a reconstructed simulated cylindrical phantom with two small cold inserts. In the second simulation study, visual detection of lesions by several observers is assessed. The third study is a quantitative analysis of the experimental data acquired using an anthropomorphic striatal phantom.

II. MATERIALS AND METHODS

A. The OSEM-R method

As mentioned previously, the technique proposed here seeks to restore the image contrast after the reconstruction has been performed. The first step of the process consists of a standard OSEM reconstruction without collimator blurring correction (OSEM-1D), and the second step consists of an expectation maximization (EM) postreconstruction restoration. We named the whole process OSEM-R (OSEM-1D with EM spatial Restoration).

The restoration procedure may be described as follows: consider a three-dimensional radioactive source, and let $i=1,\ldots,J$ be the discretization of the source object space into voxels, and n_i the true activity of the ith voxel of the object. Now, consider the reconstructed image of this object. Let $j=1,\ldots,J$ be the discretization of the image space into voxels, and N_j the reconstructed activity of the jth voxel after OSEM reconstruction. We may consider that N is a blurred reconstruction of the object n. The PSF of the imaging system corresponds to the blurring operator allowing us to estimate N from n. Since the resolution in the SPECT image varies depending on the position of the object in the field of view (FOV) of the camera, theoretically the PSF should be modeled with a nonstationary kernel and calculated at each location of the image. Let α_{ij} be the local PSF centered at point i and measured at point j. Then, we have

$$N_j = \sum_i \alpha_{ij} n_i. \tag{1}$$

The problem of image restoration is to estimate the activity n of the source from both its blurred reconstructed image N (achieved with the OSEM-1D) and the regional PSF α of the imaging system. We used the maximum likelihood by expectation maximization (ML-EM) iterative algorithm to solve this problem, according to the formula

$$\langle n_k\rangle^{(t+1)} = \frac{\langle n_k\rangle^{(t)}}{\sum_j \alpha_{kj}} \sum_j \left(\frac{\alpha_{kj} N_j}{\sum_i \langle n_i\rangle^{(t)} \alpha_{ij}} \right), \tag{2}$$

with $\langle n_k\rangle^{(t+1)}$ the reconstructed activity of the kth voxel at the $(t+1)$th iteration.

Note that this formula is similar to the ML-EM formula used in 3D volume reconstruction from the 2D projections

set,[27] but here, the problem is completely different. It is not a reconstruction from projections, but a 3D spatial restoration from reconstructed data.

1. Implementation of the algorithm

The accurate determination of the local PSF (α coefficients) would be a crucial point when using our method in the majority of clinical applications. However, in striatal imaging, the region of interest is always located near the center of the FOV, so in this clinical application, a commonly used approximation is to assume that the PSF is spatially invariant and well modeled by an isotropic Gaussian kernel.[31] Therefore in this paper, both in simulations and experimental studies, we approximate the global PSF by a stationary 3D isotropic Gaussian distribution.

The problem of the determination of the full width at half maximum (FWHM) of the PSF corresponds to the problem of the determination of the tomographic system resolution. This is generally made from the acquisition of a point or a line source placed at the center of rotation of the camera, for a given value of the radius of rotation.[32] This approach is suitable to characterize and compare system performances, but it is not clear that it is well adapted for measuring the true tomographic FWHM in a real context, when a more complex object is imaged. Indeed, when an iterative reconstruction method is used, the degree by which the reconstructed image converges to the "truth" with iteration (which directly influences this image resolution) depends on the overall complexity of the reconstructed object. Thus in this paper, we tested different FWHM close to the tomographic system resolution calculated at the center of rotation, according to the formula described in the next paragraph about the variable FWHM calculation used in OSEM-3D.

B. Reconstruction methods used in comparative study

In this paper, we test three OSEM-type reconstruction methods. The first one, called OSEM-1D, is an OSEM reconstruction without any collimator blurring correction. The second method, which we will refer to as OSEM-3D, accounts for the variable PSF of the system (collimator and detector), computed in three dimensions. In this method, the algorithm uses a symmetric projection/backprojection operator pair. The third method is our proposed OSEM-R technique. Since the first two approaches may be considered standard, they will be used to evaluate the ability of our method to achieve good spatial restoration.

The majority of previous studies with OSEM-3D have looked at the results after only a few iterations of the algorithm. However, some authors have pursued the use of tens to 100 iterations, as for example in 131-I and 18-FDG quantitative studies.[33–35] In such investigations, the total reconstructed strength within a focal volume approaches an asymptote as the number of iterations increases. One study, however, reported that the maximum reconstructed strength (i.e., the maximum standard uptake value) was still rising, even after 40 iterations.[36] Our comparisons were performed using the OSEM-3D reconstructions with only a small number of iterations, similar to what is usually used in "standard" clinical studies. In the majority of cases we used 3 iterations 15 subsets (45 iterative updates) for each reconstruction method, except the first study where the number of iterations was variable.

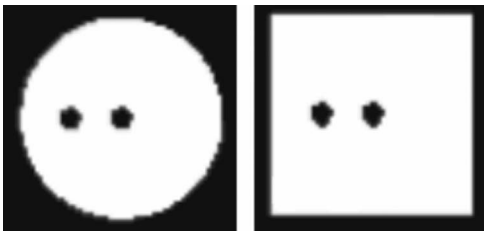

FIG. 1. Phantom number 1. Transverse and coronal slices.

For OSEM-3D, the system resolution (R_s) was calculated, at each detector-source distance according the formula $R_s=(R_c^2+R_i^2)^{0.5}$, where R_c is the collimator resolution, depending on the detector-source distance, and R_i is the intrinsic resolution. R_c was calculated using the formula $R_c=d*e/H$, where d is the detector-source distance, H is the collimator thickness, and e is the hole diameter.[1]

C. Experiments

1. Numerical phantom number 1 (for noise and contrast study)

In the first simulation study, we used a numerical phantom proposed by Kamphuis *et al.*[20] consisting of a cylinder (22 cm in diameter, 22 cm in height) filled with homogeneous activity and including two identical spheres (2.4 cm in diameter) without activity, one at the center of field, the other one eccentrically positioned at 5.5 cm from the center of the cylinder (Fig. 1).

The projections were simulated taking into account the depth-dependent resolution of the detector and Poisson noise. Attenuation and scatter were not considered. The size of the projection bin was 3.44×3.44 mm, and voxel size in the reconstructed image was $3.44\times3.44\times3.44$ mm. The physical parameters of the simulation were as follows. The low energy high resolution (LEHR) collimator was used with the geometrical resolution FWHM at 100 mm from the collimator surface equal to 8 mm, the hole size, the septal thickness, and the height of the collimator were equal to 2.0, 0.2, and 35 mm, respectively. The intrinsic camera resolution was set to 3.4 mm and the radius of rotation of the camera was equal to 130 mm. The matrix size was 64×64 and 60 projections acquired over a 360° rotation were simulated with a total of 7×10^6 counts in the study (comparable to a brain acquisition statistics). The system resolution at the center of rotation was 10.6 mm. The OSEM-R method was tested using two different FWHMs: 11 and 13 mm.

This phantom allowed us to test the performance of the algorithms by studying the contrast and the noise in the reconstructed images as a function of the number of iterations. The contrast in the image was defined by the formula

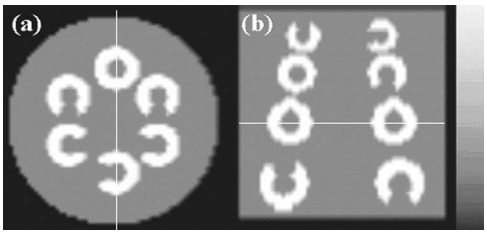

FIG. 2. (a) A transaxial slice and (b) a sagittal slice of the phantom number 2.

$$C = \frac{\lambda_{\text{hom}} - \lambda_{\text{sphere}}}{\lambda_{\text{hom}}}, \tag{3}$$

where λ_{sphere} was the mean value in a $3 \times 3 \times 3$ voxel region at the center of a cold sphere (7 pixels diam) and λ_{hom} was the mean value in a $3 \times 3 \times 3$ voxel region containing homogeneous activity. The noise was calculated inside a homogeneous transverse slice of the phantom, and was expressed in terms of a standard deviation of the activity in the slice.

2. Numerical phantom number 2 (for study of visual detection of defects)

A second numerical simulation used a phantom containing a series of small objects that provided a more accurate test of the visual detection of perfusion defects. It consisted of a 20 cm diameter and 20 cm height cylinder (Fig. 2), with a uniform background activity and four layers of six hollow spheres. In each layer, the diameters of the spheres were the same, and increased from the top to the bottom of the cylinder (respectively, 3.1, 3.6, 4.1, and 4.6 cm from first to last layer). All the spheres were filled with the same activity, which was two times higher than the background activity. These spheres were hollow at the center and opened on one side, in order to simulate a perfusion defect containing background activity, as shown in Fig. 2. The sizes of the defects were equal to a quarter of the diameter of the spheres (0.77, 0.90, 1.02, and 1.15 cm), and the location of the defect (top, bottom, left, or right) was randomly determined.

Projections were simulated including the effect of collimator blurring (the same blurring as for numerical phantom number 1), but not attenuation and Compton scatter. Poisson noise was added to the projections in order to create the signal-to-noise ratio corresponding to a 20×10^6 counts in each study.

This phantom was simulated three times having different orientations of the defects in each simulation. A total of 60 projections were simulated over 360°, with the same acquisition parameters as in the first study.

All numerical phantoms were reconstructed using the three reconstruction methods: (a) OSEM-1D (15 subsets, 3 iterations), (b) OSEM-3D (15 subsets, 3 iterations), and (c) OSEM-R (15 subsets, 3 OSEM-1D iterations followed by 3 ML-EM restoration iterations). The number of iterations and number of subsets in these reconstructions were equal to those routinely used in our clinical brain studies.

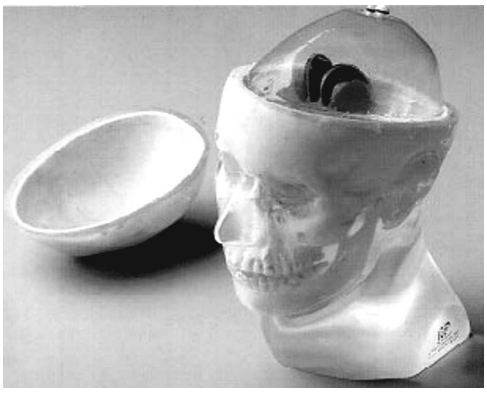

FIG. 3. Anthropomorphic head phantom used for the experimental study (Radiology Support Devices, Long Beach, CA 90810).

Reconstructed images were presented to four observers, whose task was to detect the location (top, bottom, right, left) of the defects for each of 72 spheres (18 spheres of each size: three phantoms and six identical size spheres by phantom, four layers by phantom), in both transaxial and sagittal slices. The ratio of right answers to the total number of tests has been computed for each of the defect sizes.

3. Physical radiology support device phantom (for quantitative study)

The experimental study used the radiology support device (RSD) striatal phantom (Fig. 3). The projection data were acquired using a Philips three-headed gamma camera, equipped with parallel LEHR collimators. A total of 120 angular views, equally spaced over 360°, were acquired for 10 s per view, and the projection data were sampled on a 128×128 grid with pixels of size 2.34 mm $\times$ 2.34 mm. The rotation radius was 130 mm. The theoretical system resolution at the center of rotation was 8.6 mm. The FWHM used in the OSEM-R method was 9 mm.

Chambers of the brain phantom were filled with different concentrations of 123-I. The main brain chamber contained 25.7 kBq/ml; the left caudate nucleus, 207 kBq/ml; the right caudate nucleus, 116 kBq/ml; the left putamen, 57.7 kBq/ml; and the right putamen, 28.8 kBq/ml. Three energy windows were used to perform scatter correction using the Ogawa method:[37] 136 keV±5%, 159 keV±10%, 185 keV±5%. The total number of counts was: 2.4×10^6, 9.7×10^6, and 2.2×10^6 of counts, respectively, for the three windows.

Attenuation and partial volume effect corrections were done to quantify the binding potential (BP) ratios. The BP ratio is defined by $(S\text{-NS})/\text{NS}$, where S is the striatal activity, and NS is the nonspecific brain activity, measured in the occipital region. The volume of interest (VOI) of caudate nucleus and putamens, right and left, were obtained from a 3D segmentation of computerized tomography (CT) imaging of the phantom, and the VOI for the nonspecific activity corresponded to two spherical regions positioned in the occipital area. Attenuation correction was done using the attenuation map estimated from the CT transmission scan of

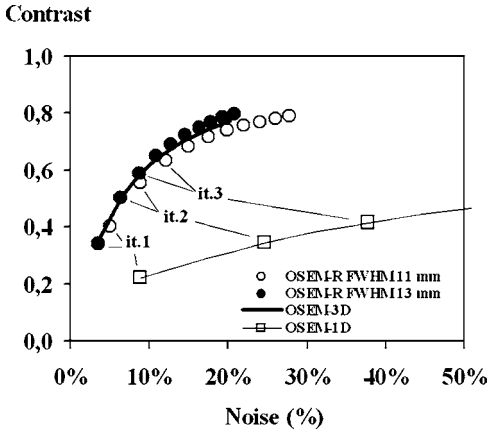

FIG. 4. Contrast as a function of noise with the increase of the number of iterations for reconstructions of the simulated phantom number 1.

the phantom. The attenuation volume was first registered with the SPECT images before being incorporated into the iterative reconstruction process.[38] The CT-SPECT registration was performed using our own rigid-body registration software. The performance of the three methods, OSEM-R, OSEM-3D, and OSEM-1D methods was tested.

For the partial volume effect correction we used a matrix inversion method based on the technique proposed by Rousset *et al.*[39] and used in Soret *et al.*[40] In this method, the partial volume correction is applied to the reconstructed data. Even after the resolution recovery correction is performed, as is the case in the OSEM-3D or OSEM-R reconstructions, partial volume correction must be applied in order to restore the correct activities in the small structures. The matrix inversion method assumes that the activity is uniformly distributed in each structure of the object and that the 3D reconstructed image of the object can be described as a sum of the elementary structures convolved by the PSF of the imaging system. So the measured activity (a_s) in a VOI corresponding to the structure s, is the result of a weighted sum of the real activity (A'_s) of all structures s'. The weighted coefficients k are calculated from the exact morphology of each structure of the object and from the PSF of the system.

$$a_s = \sum_{s'} k_{ss'} A'_s \tag{4}$$

In matrix notation, we have

$$a = kA. \tag{5}$$

This linear system is well conditioned, and the matrix k can be easily inverted. So the real activity can be obtained from the measured counts in all VOI:

$$A = k^{-1}a. \tag{6}$$

III. RESULTS

Figure 4 presents the change of contrast and noise in the image with the number of iterations in the reconstructed images of the first simulated phantom for OSEM-1D, OSEM-3D, and OSEM-R. The OSEM-R method using a PSF with FWHM between 11 and 13 mm produces image quality similar to OSEM-3D.

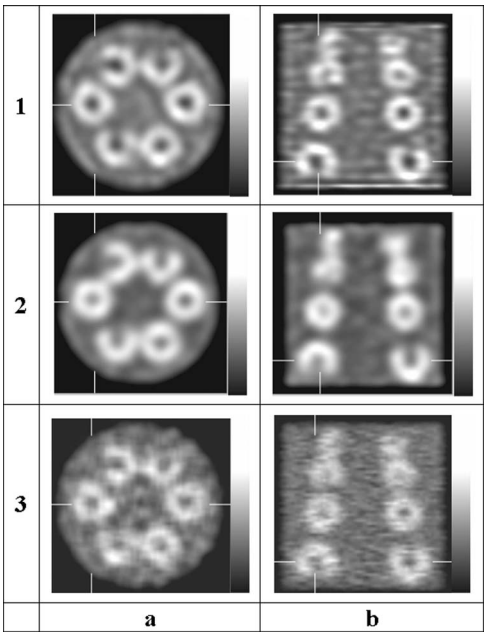

FIG. 5. Images of (a) transaxial and (b) sagittal slices of the phantom with small spheres reconstructed with: (1) OSEM-3D, (2) OSEM-R, (3) OSEM-1D.

Three examples of images of the phantom number 2 reconstructed using the same three methods are presented in Fig. 5.

Figure 6 shows the results of the human observer test of visual quality of images. Both OSEM-R and OSEM-3D reconstructions resulted in a very similar visual resolution. The percentage of correctly identified small defects by the four observers was as follows [for each defect size, the ratio (OSEM-R/OSEM-3D) gives the percentage of successes for the two methods]: 8 mm defects [37.5%/36.5%], 9 mm defects [80.2%/85.4%], 10 mm defects [100%/98.9%].

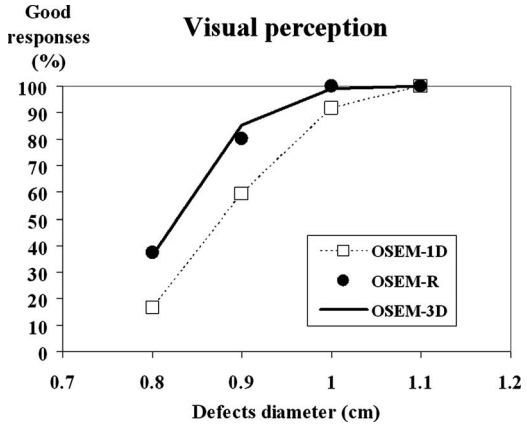

FIG. 6. Results of the visual test of defect detection for reconstruction method, depending on the diameter of the defects.

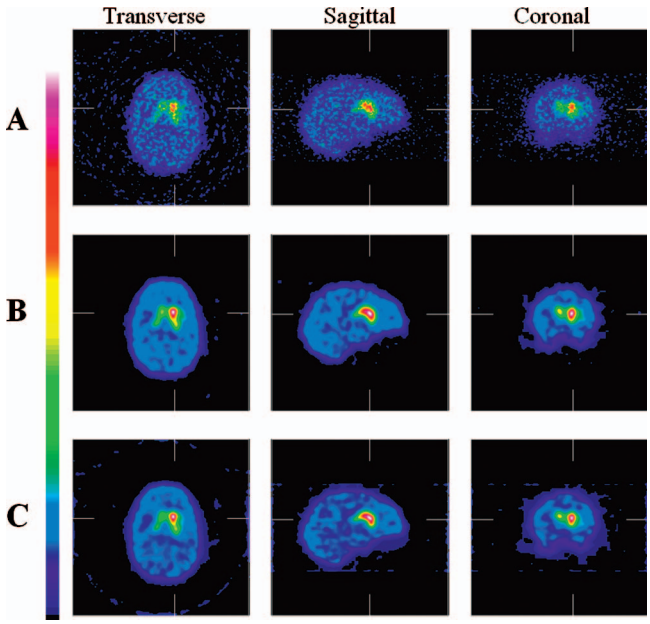

FIG. 7. Transverse, sagittal, and coronal slices of the anthropomorphic striatal phantom, reconstructed using A, OSEM-1D; B, OSEM-R; and C, OSEM-3D.

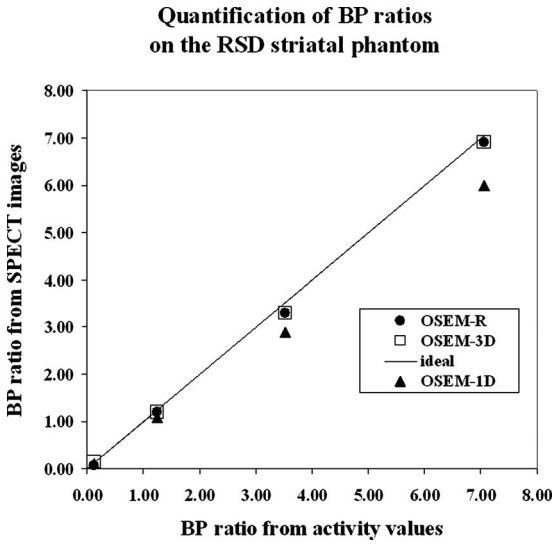

FIG. 8. The results of the quantification of the binding potential ratio (S-NS)/NS (S: striatum activity, NS: cerebellum activity) obtained from images reconstructed with the OSEM-R, OSEM-3D, and OSEM-1D methods.

Figure 7 shows three examples of the reconstructed slices of the anthropomorphic striatal phantom The OSEM-R and OSEM-3D methods give comparable images. The quantification results of the experimental study are shown in Figure 8 and Table I. Analyzing the BP ratios we did not observed any differences between the OSEM-3D and OSEM-R methods, and the BP values were close to the ideal BP (calculated from the real activities) (R^2=0.9994). Moreover, Table I shows how the FWHM used in OSEM-R influences the accuracy of quantification. Very few differences were observed between the results corresponding to different FWHM values, namely: 7, 9, and 11 mm.

IV. DISCUSSION

In this paper we present an iterative postreconstruction method to restore the resolution of the SPECT images. Our restoration approach may be considered to be an extension of the work of Richardson,[41] who has proposed an iterative algorithm for image restoration based on the conditional probability of emission and detection of photons in 2D astronomical images. Our algorithm restores resolution in 3D SPECT images, and is based on the ML-EM iterative formula. ML-EM is known to perform well when reconstructing an image from the projection data that follow the Poisson statistics.[27] Although SPECT projections do follow Poisson statistics, the same does not apply to the reconstructed images. Barret *et al.*[42] and Wilson *et al.*[43] have investigated the statistics of the images reconstructed with ML-EM and found it to be close to the log-normal distribution with the variance increasing fast during the initial iterations and then stabilizing. More importantly, this variance is low in the region of weak signal and increases in areas with strong signal. Poisson statistics displays very similar behavior, although the value of the variance is different. Therefore in this paper we have used a modified version of the ML-EM algorithm for the postreconstruction resolution recovery although we are aware that the data do not strictly follow Poisson statistics.

The proposed algorithm has several interesting properties. The positivity of the data is always maintained during iterations, because the algorithm is multiplicative. Additionally,

TABLE I. Reconstructed activity and binding potential for each of the striatal structures (RC: right caudate, LC: left caudate, RP: right putamen, LP: left putamen, NS: nonspecific occipital region), for different reconstruction method. For the OSEM-R method, three FWHM: 7, 9, and 11 mm were tested.

	Activity (kCts/ml)					BP=(S-NS)/NS no corrected				BP=(S-NS)/NS corrected of PVE			
	RC	LC	RP	LP	NS	RC	LC	RP	LP	RC	LC	RP	LP
Ideal	116	207	28.8	57.7	25.7	3.52	7.06	0.12	1.24	3.52	7.06	0.12	1.24
OSEM-3D	111	206	29.7	58.1	25.7	1.35	3.06	0.17	0.77	3.26	6.91	0.14	1.23
OSEM-1D	96.7	174	27.6	52.8	24.5	1.23	2.60	0.17	0.74	2.91	6.03	0.11	1.13
OSEM-R 9 mm	107	194	26.4	54.5	24.2	1.39	3.00	0.14	0.78	3.35	6.92	0.08	1.22
OSEM-R 7 mm	105	188	26.1	53.0	24.2	1.41	2.95	0.13	0.76	3.31	6.70	0.07	1.16
OSEM-R 11 mm	105	196	26.6	56.6	24.2	1.32	2.95	0.16	0.81	3.27	6.99	0.08	1.31

the activity in the restored volume remains constant and equal to the initial activity. These characteristics are particularly advantageous for quantitation of the data, contrary to the filtering method (using, for example, the Wiener filter). Filters, which are widely available on SPECT systems, may sometimes produce resolution results close to those obtained from the Bayesian reconstructions. They are, however, inappropriate for quantitative analysis of the images, as they tend to alter the values of activity depending on the frequency components present in the initial image. Only normalization of the total number of counts can partly compensate for this problem. Our method does not require any normalization. More importantly it performs well with noisy data, contrary to filters, which usually increase contrast only at the expense of increased noise.

Additionally, postreconstruction filters assume that resolution loss is a linear process that is translationally invariant, while in reality resolution degrades with depth in the body with anisotropic distribution of the PSF. All these effects can be taken into account when iterative methods are used because parameters α_{ij} in Eq. (2) may be set to be spatially variant. In our paper we have used the spatially invariant parameter α_{ij}, approximated by the 3D Gaussian function. This approximation is well justified for an object near the center of rotation of the camera, because in this area the resolution remains almost constant (for example, for a HRBE collimator, the system resolution varies only of 2.1 mm between 160 and 120 mm of the source-detector distance). For other applications, such as, for example, tomographic bone studies, it is possible to incorporate spatial variations of the PSF into the algorithm.

We have shown that the images reconstructed with our OSEM-R method are close to those obtained from the reference method OSEM-3D. Comparison included the analysis of the relationship between contrast recovery and noise in the data, visual detectability of the small defects, and quantitation of the activity in the striata.

The most important advantage of the OSEM-R over OSEM-3D is related to the calculation time. Assuming the same number of iterations, it is possible to estimate the number of elementary operations that are necessary to calculate projector/backprojector pair for each of the methods. This number is proportional to

(1) OSEM-1D: $D^3 2P$,
(2) OSEM-3D: $D^3 P(\gamma R)^2$,
(3) OSEM-R: $D^3[2P+(\gamma R)^3]$ for spatial domain calculation,

where D is the image size, P the number of projections, R an average resolution expressed in pixels, and γR corresponds to the number of points that need to be taken into account when calculating the PSF ($\gamma=2.1$ for a Gaussian distribution including up to 5% of the maximum). The factor of 2 in the formula for OSEM-1D and OSEM-R results from the fact that the projection of a voxel generally expands over two pixels in the detection plane (central radius approximation).

If one considers the invariance of the PSF, it is possible to accelerate the calculation of the iterative formula of the restoration process of OSEM-R by using the Fourier transform to calculate the terms $C_i=\Sigma_i\langle n_i\rangle^{(t)}\alpha_{ij}$ and $\Sigma_j\alpha_{kj}N_j/C_i$ of the formula (2), which correspond to convolutions. Note that this technique using the Fourier transform to calculate the iterative formula of EM restoration, should not be compared to the deconvolution filtering techniques that also employ the Fourier transform. Although the EM restoration in the frequency domain should not be used with the spatially variant PSF, with the constant PSF it gives the same results that a spatial convolution, with less time calculation. In this case, the number of operations of OSEM-R is proportional to

OSEM-R: $D^3[2P+(\beta R)]$ for frequency domain calculation.

In our experiment we found β close to 1.93.

The relative gain of the calculation time required by OSEM-R as compared to that of OSEM-3D can be approximated by the formulas

$$G_{\text{spat}} \approx \frac{P(\gamma R)^2}{2P+(\gamma R)^3} \quad \text{and} \quad G_{\text{freq}} \approx \frac{P(\gamma R)^2}{2P+(\beta R)}.$$

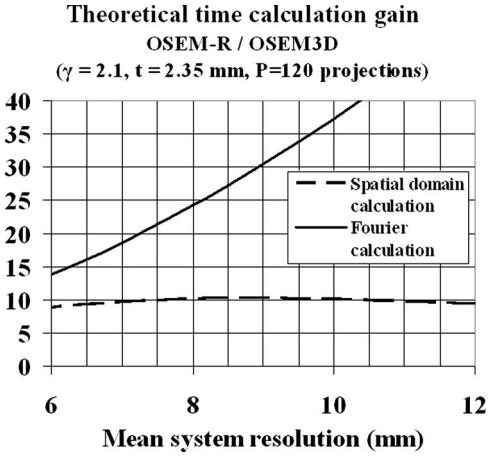

FIG. 9. Theoretical estimate of the decrease of the calculation time obtained with OSEM-R compared to OSEM-3D as a function of mean system resolution expressed in millimeters for pixel size 2.35 mm, and 120 projections. For the restoration step of the OSEM-R method, two techniques were analyzed: one using a spatial domain calculation and the second using a frequency domain calculation.

Figure 9 presents the ratios of the calculation time required for the OSEM-R relative to the OSEM-3D method obtained from these theoretical formulas. The estimation was performed for a series of system resolutions expressed in millimeters, for $P=120$, $\gamma=2.1$, pixel size $t=2.35$ mm, and $\beta=1.93$. Obviously, the system resolution will depend on the collimator type and radius of rotation of the camera.

Table II gives an example of measured calculation times, when using a PC Pentium IV 3.4 GHz computer, to reconstruct clinical images of neurotransmission. In these experiments, the complete OSEM-R reconstructions were 3 min 2 s+2 min 55 s=5 min 57′ s, and 3 min 2 s+6 s =3 min 8 s for, respectively, spatial and frequency domain

TABLE II. Example of calculation times for reconstructions from 120 projections, using a 128×128 matrix, 2.35 mm pixels, LEHR collimator, FWHM: 9 mm at the center of rotation, 3 iterations with 15 subsets.

	OSEM-3D	OSEM-1D	EM restoration in spatial domain	EM restoration in frequency domain
Calculation time for 3 iterations	1 h 18 min	3 min 2 s	2 min 55 s	6 s

calculations. The experimental OSEM-R/OSEM-3D gains were equal, respectively, to: 13 and 25, while theoretically estimated gain should be close to 10 and 30.

V. CONCLUSION

We have demonstrated that, in neurotransmission brain study, an iterative ML-EM postreconstruction invariant restoration method may be a valuable alternative to the OSEM-3D reconstruction including spatially variant resolution correction within the reconstruction process. Both methods resulted in comparable image quality while the OSEM-R method is much faster. In a future study, we will investigate a spatially variant model for the PSF. This approach will allow us to take into account the variation of the collimator resolution with depth, and include it into the restoration process of OSEM-R in order to be able to apply this method to imaging other organs.

[1]H. O. Anger, "Scintillation camera with multichannel collimators," J. Nucl. Med. **65**, 515–531 (1964).
[2]E. J. Hoffman, S. C. Huang, and M. E. Phelps, "Quantitation in positron emission computed tomography: Effect of object size," J. Comput. Assist. Tomogr. **3**, 299–308 (1979).
[3]A. Kojima, M. Matsumoto, M. Takahashi, Y. Hiota, and H. Yoshida, "Effect of spatial resolution on SPECT quantification values," J. Nucl. Med. **30**, 508–514 (1989).
[4]M. A. King, D. T. Long, and A. B. Bill, "SPECT volume quantitation influence of spatial resolution, source size and shape, and voxel size," Med. Phys. **18**, 1016–1024 (1991).
[5]P. H. Pretorius, M. A. King, T. S. Pan, D. J. de Vries, S. J. Glick, and C. L. Byrne, "Reducing the influence of the partial volume effect on SPECT activity quantitation with 3D modelling of spatial resolution in iterative reconstruction," Phys. Med. Biol. **43**, 407–420 (1998).
[6]M. T. Madsen and C. H. Park, "Enhancement of SPECT images by Fourier filtering the projection image set," J. Nucl. Med. **26**, 395–402 (1979).
[7]M. A. King, R. B. Schwinger, R. W. Doherty, and B. C. Penney, "Two-dimensional filtering of SPECT images using the Metz and Wiener filters," J. Nucl. Med. **25**, 1234–1240 (1984).
[8]D. R. Gilland, B. M. Tsui, W. H. McCartney, J. R. Perry, and J. Berg, "Determination of the optimum filter function for SPECT imaging," J. Nucl. Med. **29**, 643–650 (1988).
[9]T. C. Hon, R. M. Rangayyan, L. J. Hahn, and R. Kloiber, "Restoration of gamma camera-based nuclear medicine images," IEEE Trans. Med. Imaging **8**, 354–363 (1989).
[10]B. C. Penney, M. A. King, R. B. Schwinger, S. P. Baker, and P. W. Doherty, "Modifying constrained least-squares restoration for application to single photon emission computed tomography projection images," Med. Phys. **15**, 334–342 (1988).
[11]L. van Elmbt and S. Walrand, "Simultaneous correction of attenuation and distance-dependent resolution in SPECT: an analytical approach," Phys. Med. Biol. **38**, 1207–1217 (1993).
[12]J. M. Franquiz and S. Shukla, "A multiresolution restoration method for cardiac SPECT imaging," Med. Phys. **25**, 2469–2475 (1998).
[13]R. M. Lewitt, P. R. Edholm, and W. Xia, "Fourier method for correction of depth-dependent collimator blurring," Proc SPIE Medical Imaging III image processing, 232–243 (1989).
[14]S. J. Glick, B. C. Penney, M. A. King, and C. L. Byrne, "Non iterative compensation for the distance-dependent detector response and photon attenuation in SPECT imaging," IEEE Trans. Med. Imaging **13**, 363–374 (1994).
[15]W. Xia, R. M. Lewitt, and P. R. Edholm, "Fourier correction for spatially variant collimator blurring in SPECT," IEEE Trans. Med. Imaging **14**, 100–115 (1995).
[16]V. Kohli, M. A. King, S. J. Glick, and T. S. Pan, "Comparison of frequency-distance relationship and Gaussian-diffusion based methods of compensation for distance-dependent spatial resolution in SPECT imaging," Phys. Med. Biol. **43**, 1025–1037 (1998).
[17]B. M. W. Tsui, H. B. Hu, D. R. Gilland, and G. T. Gullberg, "Implementation of simultaneous attenuation and detector response correction in SPECT," IEEE Trans. Nucl. Sci. **35**, 778–783 (1988).
[18]A. R. Formiconi, A. Pupi, and A. Passeri, "Compensation of spatial system response in SPECT with conjugate gradient reconstruction technique," Phys. Med. Biol. **34**, 69–84 (1989).
[19]G. L. Zeng, G. T. Gullberg, B. M. W. Tsui, and J. A. Terry, "Three-dimensional iterative reconstruction algorithms with attenuation and geometric point response correction," IEEE Trans. Nucl. Sci. **38**, 693–702 (1991).
[20]C. Kamphuis, F. J. Beekman, and M. A. Viergever, "Evaluation of OS-EM vs ML-EM for 1D, 2D, and fully 3D SPECT reconstruction," IEEE Trans. Nucl. Sci. **43**, 2018–2024 (1996).
[21]B. F. Hutton and Y. H. Lau, "Application of distance-dependent resolution compensation and post-reconstruction filtering for myocardial SPECT," Phys. Med. Biol. **43**, 1679–1693 (1998).
[22]G. L. Zeng and G. T. Gullberg, "Frequency domain implementation of the three-dimensional geometric point response correction in SPECT imaging," IEEE Trans. Nucl. Sci. **39**, 1444–1453 (1992).
[23]G. L. Zeng and G. T. Gullberg, "Unmatched projector/backprojector pairs in an iterative reconstruction algorithm," IEEE Trans. Med. Imaging **19**, 548–555 (2000).
[24]D. Boulfelfel, R. M. Rangayyan, L. J. Hahn, and R. Kloiber, "Three-dimensional restoration of single photon emission computed tomography images," IEEE Trans. Nucl. Sci. **41**, 1746–1754 (1994).
[25]S. Webb, A. P. Long, R. J. Ott, M. O. Leach, and M. A. Flower, "Constrained deconvolution of SPECT liver tomograms by direct digital image restoration," Med. Phys. **12**, 53–58 (1985).
[26]M. Mignotte and J. Meunier, "Three-dimensional blind deconvolution of SPECT images," IEEE Trans. Biomed. Eng. **47**, 274–280 (2000).
[27]L. A. Shepp and Y. Vardi, "Maximum likelihood reconstruction for emission tomography," IEEE Trans. Med. Imaging **1**, 113–122 (1982).
[28]H. M. Hudson and R. S. Larkin, "Accelerated image reconstruction using ordered subsets of projection data," IEEE Trans. Med. Imaging **13**, 601–609 (1994).
[29]R. G. Wells *et al.*, "Comparing filtered backprojection and ordered-subsets expectation maximization for small-lesion detection and localization in 67 Ga SPECT," J. Nucl. Med. **41**, 1391–1399 (2000).
[30]H. C. Gifford, M. A. King, R. G. Wells, W. G. Hawkins, M. V. Narayanan, and P. H. Pretorius, "LROC analysis of detector-response compensation in SPECT," IEEE Trans. Med. Imaging **19**, 463–473 (2000).
[31]V. Frouin, C. Comtat, A. Reilhac, and M. C. Gregoire, "Correction of partial-volume effect for PET striatal imaging: fast implementation and study of robustness," J. Nucl. Med. **43**, 1715–1726 (2002).
[32]NEMA Standards publication NU 1-2001, Performance measurements of scintillation cameras, National Electrical Manufacturers Association, Rosslyn, VA USA
[33]K. F. Koral, Q. Lin, A. Yendiki, Y. K. Dewaraja, and J. A. Fessler, "Determining Total I-131 activity within a VoI using SPECT, a UHE collimator, OSEM and a constant conversion factor," IEEE Trans. Nucl. Sci.

51, 611–618 (2004).
[34]K. F. Koral, A. Yendiki, Q. Lin, and Y. K. Dewaraja, "Comparison of 3D OSEM vs 1D SAGE for focal total-activity quantification in I-131 SPECT with HE collimation," IEEE Trans. Nucl. Sci. **52**, 154–158 (2005).
[35]Y. K. Dewaraja, S. J. Wilderman, M. Ljungberg, K. F. Koral, K. Zasadny, and M. Kaminski, "Accurate dosimetry in I-131 radionuclide therapy using patient specific, 3-dimensional methods for SPECT reconstruction and absorbed dose calculation," J. Nucl. Med. **46**, 840–849 (2005).
[36]C. J. Jaskowiak, J. A. Bianco, S. B. Perlman, and J. P. Fine, "Influence of reconstruction iterations on 18-F-FDG PET/CT standardized uptake values," J. Nucl. Med. **46**, 424–428 (2005).
[37]K. Ogawa, Y. Harata, T. Ichihara, A. Kubo, and S. Hashimoto, "A practical method for position-dependent Compton-scatter correction in single photon emission CT," IEEE Trans. Med. Imaging **10**, 408–412 (1991).
[38]G. T. Gullberg, R. H. Huesman, J. A. Malko, N. J. Pelc, and T. F. Budinger, "An attenuated projector-backprojector for iterative SPECT reconstruction," Phys. Med. Biol. **30**, 799–816 (1985).
[39]O. G. Rousset, Y. Ma, and A. C. Evans, "Correction for partial volume effects in PET: principle and validation," J. Nucl. Med. **39**, 904–911 (1998).
[40]M. Soret, P. M. Koulibaly, J. Darcourt, S. Hapdey, and I. Buvat, "Quantitative accuracy of dopaminergic neurotransmission imaging with (123)I SPECT," J. Nucl. Med. **44**, 1184–1193 (2003).
[41]W. H. Richardson, "Bayesian-based iterative method of image restoration," J. Opt. Soc. Am. **62**, 55–59 (1972).
[42]H. H. Barrett, D. W. Wilson, and B. M. W. Tsui, "Noise properties of the EM algorithm. I. Theory," Phys. Med. Biol. **39**, 833–846 (1994).
[43]D. W. Wilson, B. M. W. Tsui, and H. H. Barrett, "Noise properties of the EM algorithm. II. Monte Carlo simulations," Phys. Med. Biol. **39**, 847–871 (1994).